Diffractive open charm production at DESY HERA: experiment versus two-gluon exchange model

S.P. Baranov*
P.N. Lebedev Institute of Physics, Leninsky prosp. 53, Moscow 119991, Russia
(Dated: March 20, 2010)

Diffractive production of D^* mesons at HERA conditions is considered in the framework of collinear two-gluon exchange model. Theoretical results are compared with recent experimental data.

PACS numbers: 12.38.Bx, 13.60.-r, 13.60.Le

I. INTRODUCTION

Nowadays, the interpretation of diffractive processes in high energy particle collisions in terms of the two-gluon exchange mechanism is widely discussed in the literature. This approach has already demonstrated its capability to describe a large range of experimental data, and it provides attractive theoretical grounds for deriving further predictions for running and planned experiments.

The present work is devoted to a detailed comparison between theoretical calculations and recent experimental data collected by the HERA collaborations H1 [1] and ZEUS [2, 3] on inclusive diffractive production of D^* mesons. Each of the two collaborations have explored both the real photoproduction and the deep-inelastic regimes, so that in total there are four sets of experimental data.

Within the two-gluon exchange model, calculations for the diffractive production of unbound heavy quark states $Q\bar{Q}$ have been reported in [4], but this process is found to bring only a minor contribution at the experimental conditions under study. In Ref. [5], the production of massless quark pairs with an additional gluon in the final state $q\bar{q}g$ has been considered, and later on this approach has been extended to the massive $Q\bar{Q}g$ states [6]. Although a comparison with the first H1 and ZEUS data has been presented in Ref. [6], a body of new and more precise data has been collected by both collaborations since then. Apart from the theoretical results shown just in Ref. [1] (also obtained within the approach of Ref. [6]), no other comparisons with the mentioned data are known to the author. The only exception is the paper [7] which is, however, based on the "constituent" or "resolved" Pomeron picture rather than the two-gluon exchange model.

A few words are in order to clarify the difference between the approach which we are using here and that of Ref. [8]. First, we are working in the collinear scheme, while the authors of [8] prefer the k_t-factorization, where the Pomeron exchange is modeled by the unintegrated gluon distribution $\mathcal{F}_g(x_{I\!P}, k_t^2)$. In that approximation the difference of the longitudinal momenta x_1 and x_2 of the two gluons is neglected. Therefore, in contrast with our approach (see below), there is no integration over the gluon longitudinal momentum fraction, but, instead, there is integration over the gluon transverse momentum. Second, we suspect that the calculations in [8] are based on a much lower number of Feynman diagrams, a fact that potentially may cause problems with gauge invariance.

The outline of the paper is the following. In Sec. II we describe the theoretical approach used in our calculations. The evaluation of the real and imaginary parts of the two-gluon exchange amplitude is explained in every detail in Sec. III. In Sec. IV we display our numerical predictions on the different kinematic distributions along with the results of experimental measurements. Our findings are summarized in Sec. V.

II. THEORETICAL FRAMEWORK

This study focuses on the process

$$e + p \to e' + p' + D^* + X. \qquad (1)$$

The relevant kinematic variables are explained in Fig. 1.

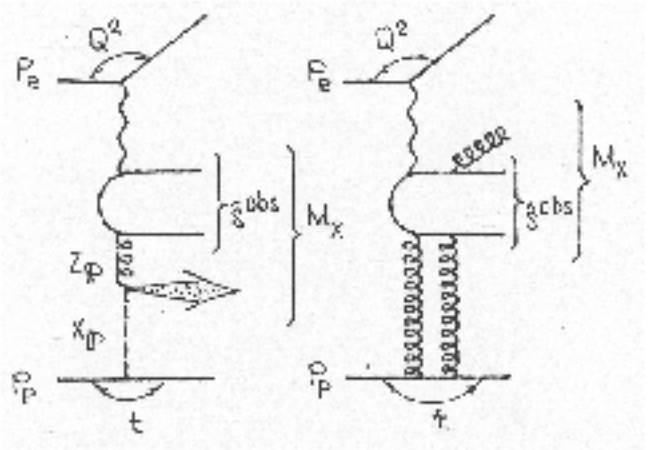

FIG. 1: Schematic representation of the reaction kinematics. Left panel, "resolved Pomeron" model; right panel, two-gluon exchange model.

*Electronic address: baranov@sci.lebedev.ru

Our calculations are based on perturbative QCD and the two-gluon exchange model with so-called skewed gluon distributions. At the parton level, we consider the subprocesses

$$\gamma^* + (gg) \to c + \bar{c} \tag{2}$$

and

$$\gamma^* + (gg) \to c + \bar{c} + g \tag{3}$$

where the notation (gg) stands for a colorless and parity-even system of two gluons carrying the longitudinal momentum fractions x_1 and x_2 with respect to the quantity $(p_p + p'_p)/2$, with p_p and p'_p being the momenta of the initial and scattered protons. Hereafter, we will refer to the subprocesses (2) and (3) as to leading order (LO) and next-to-leading (NLO) contributions. The corresponding Feynman diagrams are displayed in Figs. 2 and 3.

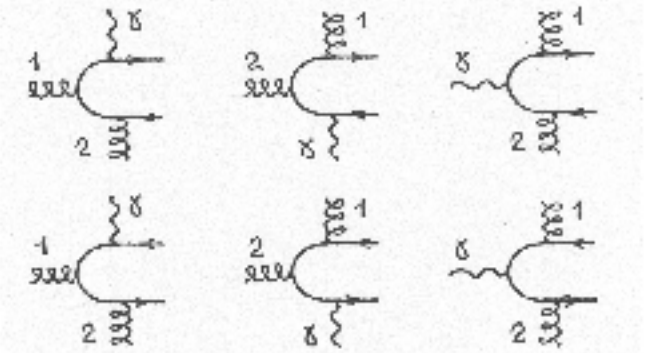

FIG. 2: Feynman diagrams representing the LO subprocess $\gamma^* + \mathbb{P} \to c + \bar{c}$. The numbers 1 and 2 indicate the initial state gluons constituting the "Pomeron".

The evaluation of the diagrams is straightforward and follows the standard QCD Feynman rules. The spin density matrix of the virtual photon is determined by the momenta p_e and p'_e of the initial and scattered electron and is represented in our calculations by the full lepton tensor

$$L^{\mu\nu} = 8\, p_e^\mu p_e^\nu - 4(p_e k_\gamma)\, g^{\mu\nu}, \tag{4}$$

with $k_\gamma = p_e - p'_e$ being the virtual photon momentum. In this way we automatically take into account the contributions from both transversely and longitudinally polarized photons, as well as the interference between them. The polarization vectors of the initial gluons constituting the "Pomeron" are defined as explicit 4-vectors. In the frame with the z axis oriented along the Pomeron momentum, the x, y, z, and t components of the gluon polarization vector are parametrized as

$$e_g^{(x,y,z,t)} = (\cos\chi,\ \sin\chi,\ 0,\ 0), \tag{5}$$

where the angle χ is taken at random for every generated event. This definition suits both the collinear and

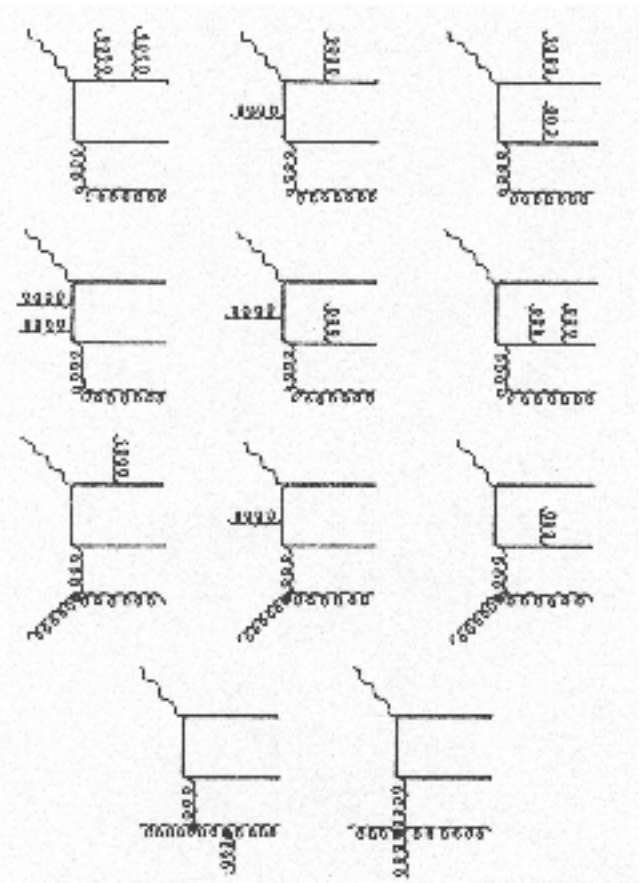

FIG. 3: Examples of Feynman diagrams representing the NLO subprocess $\gamma^* + \mathbb{P} \to c + \bar{c} + g$. The full gauge invariant set comprises 42 diagrams.

the k_t-factorization regimes. In the collinear approximation, the averaging over the random angle χ stands for the averaging over transverse polarizations of the on-shell gluons. At the same time, this definition meets the usual k_t-factorization prescription [8] $e_g^\mu = k_{gT}^\mu / |k_{gT}|$, with χ being the azimuthal angle of the gluon transverse momentum k_{gT}. The outgoing gluon in the NLO subprocess (3) is assumed to be on-shell and transversely polarized.

The evaluation of Feynman diagrams has been performed using the algebraic manipulation system FORM [9]. Managing as many as 42 interfering diagrams was not an easy technical task. To do this job we used the method of orthogonal amplitudes described in detail in Refs. [10]. The gauge invariance of the matrix elements $\mathcal{M}_{\rm LO}(\gamma^* \mathbb{P} \to c\bar{c})$ and $\mathcal{M}_{\rm NLO}(\gamma^* \mathbb{P} \to c\bar{c}g)$ of the indicated subprocesses has been explicitly tested by substituting the gluon momentum k_g^μ for the gluon polarization vector e_g^μ and, independently, by substituting the photon momentum k_γ^μ for the photon polarization vector e_γ^μ. The FORTRAN code for the matrix elements is available from the author on request.

The matrix elements of the partonic subprocesses have to be convoluted with generalized (or skewed) gluon distribution $\mathcal{H}$. Let $x_{\mathbb{P}}$ be the Pomeron momentum frac-

tion, x_1 and x_2 the gluon momentum fractions, and v and ξ the integration variables in symmetric notation [11], such that $x_1 = (\xi+v)/(1+\xi)$, $x_2 = (\xi-v)/(1+\xi)$, and $x_1 + x_2 = x_{I\!P} = 2\xi/(1+\xi)$. Then, the amplitude of the process (1) reads

$$\mathcal{A}(ep \to epD^+X) = \int_{-1}^{1} \frac{\mathcal{M}\,\mathcal{H}(v,\xi;\mu^2,t)}{(v+\xi-ie)(v-\xi+ie)}\,dv. \qquad (6)$$

In the approach which we are using here, the skewed gluon distribution $\mathcal{H}(v,\xi;\mu^2,t)$ is related to the double distribution $F_{DD}(x,y;\mu^2,t)$ [12] via the reduction integral

$$\mathcal{H}(v,\xi;\mu^2,t) = \int_{-1}^{1} dx' \int_{-1+|\xi|}^{1-|\xi|} dy'\, \delta(x'+\xi y'-v)\, F_{DD}(x',y';\mu^2,t), \qquad (7)$$

and a model for $F_{DD}(x,y;\mu^2,t)$ is introduced in [13], in which its t dependence factorizes from the x and y dependences:

$$F_{DD}(x,y;\mu^2,t) = h(x,y)\,G(x,\mu^2)\,\tau(t). \qquad (8)$$

In accord with [14], the profile function $h(x,y)$ is chosen in the form

$$h(x,y) = \frac{\Gamma(2b+2)}{2^{2b+1}\Gamma^2(b+1)}\,\frac{[(1-|x|)^2-y^2]^b}{(1-|x|)^{2b+1}}, \qquad (9)$$

normalized to $\int_{-1+|\xi|}^{1-|\xi|} h(x,y)\,dy = 1$, and with the parameter b set equal to 2 for the case of gluons. For the input gluon density $G(x,\mu^2)$ in (8), we use the parametrization of Glück-Reya-Vogt (GRV) [15]. We have checked that the resulting distribution is numerically very close to the one presented in Ref. [16].

The t dependence of the formfactor $\tau(t)$ is taken as [17]

$$\tau^2(t) = \exp(-b|t| + ct^2) \qquad (10)$$

with $b = 9.5$ GeV^{-2} and $c = 5$ GeV^{-4} [17].

The multiparticle phase space $\prod d^3p_i/(2E_i)\,\delta^4(\sum p_{in} - \sum p_{out})$ of the considered reactions $ep \to e'p'c\bar{c}$ and $ep \to e'p'c\bar{c}g$ is parametrized in terms of rapidities, transverse momenta, and azimuthal angles: $d^3p_i/(2E_i) = (\pi/2)\,dp_{iT}^2\,dy_i\,d\phi_i/(2\pi)$. Let s be the total initial invariant energy squared, $\hat{s} = (k_\gamma + p_{I\!P})^2$ the squared energy of the partonic subprocess, $Q^2 = -k_\gamma^2$ the photon virtuality, t the momentum transfer at the proton vertex, and p'_{eT}, p_{1T}, p_{2T}, ϕ_e, ϕ_1, ϕ_2, y_1, y_2, and y_g the transverse momenta, azimuthal angles and rapidities of the scattered electron, final state quark, antiquark, and coproduced gluon, respectively. Then, the fully differential cross sections read

$$d\sigma_{\rm LO}(ep \to e'p'c\bar{c}) = \frac{\alpha^2\alpha_s^2}{16\pi s^2}\,\frac{1}{Q^4}\,\frac{1}{2}\sum_{\rm spins}\,\frac{1}{64}\sum_{\rm colors}|\mathcal{A}_{\rm LO}(\gamma^* I\!P \to c\bar{c})|^2 \times \tau^2(t)\,dt\,dp_{eT}^2\,dp_{1T}^2\,dy_1\,dy_2\,\frac{d\phi_e}{2\pi}\,\frac{d\phi_1}{2\pi}, \qquad (11)$$

$$d\sigma_{\rm NLO}(ep \to e'p'c\bar{c}g) = \frac{\alpha^2\alpha_s^3}{64\pi^2 s^2}\,\frac{1}{Q^4}\,\frac{1}{2}\sum_{\rm spins}\,\frac{1}{64}\sum_{\rm colors}|\mathcal{A}_{\rm NLO}(\gamma^* I\!P \to c\bar{c}g)|^2 \times \tau^2(t)\,dt\,dp_{eT}^2\,dp_{1T}^2\,dp_{2T}^2\,dy_1\,dy_2\,dy_g\,\frac{d\phi_e}{2\pi}\,\frac{d\phi_1}{2\pi}\,\frac{d\phi_2}{2\pi}. \qquad (12)$$

The phase space physical boundary is determined by the inequalities [18]

$$G(\hat{s},t_1,s_2,-Q^2,t,0) \le 0 \quad \text{and} \quad 4m_c^2 \le s_2 \le s \qquad (13)$$

where m_c is the charmed quark mass, $t_1 = (k_\gamma - k_g)^2$, $s_2 = (p_1+p_2)^2$, and G is the standard kinematic function [18]. The multidimensional integration over the phase space has been performed by means of the Monte-Carlo technique, using the routine VEGAS [19]. Finally, the produced charmed quarks have been converted into D^+ mesons using the Peterson fragmentation function [20].

III. TECHNICAL DETAILS

In this section we present details of the calculation of the quantity (6). First, consider the leading order amplitude $\mathcal{A}_{\rm LO}$. The expression for the corresponding matrix element $\mathcal{M}_{\rm LO}$ exhibits singularities at $v = \pm\xi$. First of all, we have to factor them out. Using the symmetry of $\mathcal{M}_{\rm LO}$ and $\mathcal{H}$ with respect to $v \to -v$ we can restrict the integration interval to $[0,1]$ and rewrite Eq.(6) in the form

$$\mathcal{A}_{\rm LO} = 2\int_0^1 \frac{(v-\xi)\mathcal{M}_{\rm LO}\mathcal{H}(v,\xi)}{(v+\xi)(v-\xi+ie)^2}\,dv = \int_0^1 \frac{F(v,\xi)}{(v-\xi+ie)^2}\,dv \qquad (14)$$

with $F(v,\xi)$ being the shorthand notation for the product of the regular part of the matrix element and the skewed gluon distribution:

$$F(v,\xi) = 2\mathcal{M}_{\rm LO}\mathcal{H}(v,\xi)\,(v-\xi)/(v+\xi). \qquad (15)$$

The integrand expression contains a double pole at $v = \xi$. The real and imaginary parts of the amplitude (14) read

$$\Re e\mathcal{A}_{\rm LO} = \int_0^1 \frac{[(v-\xi)^2 - e^2]\,F(v,\xi)}{[(v-\xi)^2+e^2]^2}\,dv = \int_{-\ell}^{1-\ell} \frac{(x^2-e^2)\,F(x,\xi)}{(x^2+e^2)^2}\,dx, \qquad (16)$$

$$\Im m\mathcal{A}_{\rm LO} = -2e\int_0^1 \frac{(v-\xi)\,F(v,\xi)}{[(v-\xi)^2+e^2]^2}\,dv = -2e\int_{-\ell}^{1-\ell} \frac{x\,F(x,\xi)}{(x^2+e^2)^2}\,dx, \qquad (17)$$

where $x = v - \xi$. Now, we expand $F(x,\xi)$ in powers of x around $x = 0$:

$$F(x,\xi) = F_0 + xF_1 + F_2(x,\xi), \qquad (18)$$

where $F_0 = F(x,\xi)\big|_{x=0}$, $F_1 = \frac{d}{dx}F(x,\xi)\big|_{x=0}$, and $F_2(x,\xi) = F(x,\xi) - F_0 - xF_1$, so that $F_2(x,\xi)/x^2$ is finite at $x=0$. The term by term integration yields for the real part:

$$F_0\int_{-\ell}^{1-\ell}\frac{(x^2-e^2)}{(x^2+e^2)^2}\,dx = -F_0\,\frac{x}{(x^2+e^2)}\Big|_{-\ell}^{1-\ell} \to -F_0\frac{1}{\xi(1-\xi)}, \quad (19)$$

$$F_1\int_{-\ell}^{1-\ell}\frac{(x^2-e^2)x}{(x^2+e^2)^2}\,dx = \frac{1}{2}F_1\ln(x^2+e^2)\Big|_{-\ell}^{1-\ell} \to F_1\ln\frac{1-\xi}{\xi}, \quad (20)$$

and, for the imaginary part:

$$-2eF_0\int_{-\ell}^{1-\ell}\frac{x}{(x^2+e^2)^2}\,dx = \frac{eF_0}{x^2+e^2}\Big|_{-\ell}^{1-\ell} \to 0, \quad (21)$$

$$-2eF_1\int_{-\ell}^{1-\ell}\frac{x^2}{(x^2+e^2)^2}\,dx = -F_1\arctan\frac{x}{e}\Big|_{-\ell}^{1-\ell} \to -\pi F_1, \quad (22)$$

thus resulting in

$$\Re\mathrm{e}\mathcal{A}_{\rm LO} = -\frac{F_0}{\xi(1-\xi)} + F_1\ln\frac{1-\xi}{\xi} + \int_0^1\frac{F_2(v,\xi)}{(v-\xi)^2}\,dv \quad (23)$$

and

$$\Im\mathrm{m}\mathcal{A}_{\rm LO} = -\pi\,\frac{dF(v,\xi)}{dv}\Big|_{v=\ell}. \quad (24)$$

As it has been mentioned already, the integrand expression in the third term in (23) is finite at $v=\xi$, and so, the integration can be safely performed numerically, by means of any standard integration technique.

Now let us turn to the gluon-associated production of charm. The corresponding matrix element $\mathcal{M}_{\rm NLO}$ has singularities at $v=\pm\xi$ and also at

$$v = \pm\left\{(1+\xi)\left[(p_1k_\gamma) - k_\gamma^2\right] / \left[(k_\gamma p_p) - (p_1p_p)\right] - \xi\right\}, \quad (25)$$

and

$$v = \pm\left\{(1+\xi)(p_1k_g) / \left[(k_g p_p) + (p_1p_p)\right] - \xi\right\}. \quad (26)$$

So, the integrand expression in (6) has two double poles at $v=\pm\xi$ and four single poles as indicated in Eqs. (25),(26). Since the position of the poles is known, the full integration interval can be divided into six intervals, each containing only one singularity.

The double poles at $v=\pm\xi$ can be treated exactly in the same manner as in the previous (LO) case. So, we only have to consider the single poles. Let v_0 be the pole position and a and b the endpoints of the proper integration interval, $v_0\in[a,b]$. Then, the contribution from this particular interval to the amplitude $\mathcal{A}_{\rm NLO}$ reads

$$\mathcal{A}_{\rm NLO}^{ab} = \int_a^b\frac{\mathcal{M}_{\rm NLO}\mathcal{H}(v,\xi)}{(v+\xi)(v-\xi)}\,\frac{(v-v_0)}{(v-v_0+ie)}\,dv = \int_a^b\frac{F(v,\xi)}{(v-v_0+ie)}\,dv \quad (27)$$

with $F(v,\xi)$ being the shorthand notation for the product of the regular part of the matrix element and the skewed gluon distribution:

$$F(v,\xi) = \mathcal{M}_{\rm NLO}\mathcal{H}(v,\xi)\,(v-v_0)/[(v+\xi)(v-\xi)]. \quad (28)$$

The contributions to the real and imaginary parts of the amplitude are

$$\Re\mathrm{e}\mathcal{A}_{\rm NLO}^{ab} = \int_a^b\frac{(v-v_0)F(v,\xi)}{(v-v_0)^2+e^2}\,dv, \quad (29)$$

$$\Im\mathrm{m}\mathcal{A}_{\rm NLO}^{ab} = -\int_a^b\frac{eF(v,\xi)}{(v-v_0)^2+e^2}\,dv. \quad (30)$$

To evaluate the real part, we split the integrand function into three terms using the decomposition

$$F(v,\xi) = F_0 + (v-v_0)F_1 + F_2(v,\xi), \quad (31)$$

where $F_0 = F(v,\xi)\big|_{v=v_0}$, $F_1 = \frac{d}{dv}F(v,\xi)\big|_{v=v_0}$, and $F_2(v,\xi) = F(v,\xi) - F_0 - (v-v_0)F_1$, so that the expression for $F_2(v,\xi)/(v-v_0)$ exhibits no singularity at $v=v_0$. After performing the integration we obtain

$$F_0\int_a^b\frac{(v-v_0)}{(v-v_0)^2+e^2}\,dv = \frac{1}{2}F_0\ln\left[(v-v_0)^2+e^2\right]\Big|_a^b \to F_0\ln\left|\frac{b-v_0}{a-v_0}\right|, \quad (32)$$

$$F_1\int_a^b\frac{(v-v_0)^2}{(v-\xi)^2+e^2}\,dv \to F_1\int_a^b dv = (b-a)F_1, \quad (33)$$

thus arriving at

$$\Re\mathrm{e}\mathcal{A}_{\rm NLO}^{ab} = F_0\ln\left|\frac{b-v_0}{a-v_0}\right| + (b-a)F_1 + \int_a^b\frac{F_2(v,\xi)}{(v-v_0)}\,dv, \quad (34)$$

where the third term can be evaluated numerically by means of any standard integration technique.

Finally, to evaluate the imaginary part of the amplitude $\mathcal{A}_{\rm NLO}$ we use the property that

$$\lim_{e\to 0}\left\{e/\left[(v-v_0)^2+e^2\right]\right\} = \pi\,\delta(v-v_0), \quad (35)$$

which results in

$$\Im\mathrm{m}\mathcal{A}_{\rm NLO}^{ab} = -\pi F(v,\xi)\big|_{v=v_0}. \quad (36)$$

The contributions (24) and (36) to the imaginary part of the amplitude can be easily recognized as the residues

of the integrand expression in (14) at the isolated poles $v = \pm\xi$ and (25),(26). Note, however, that the famous formula

$$\int_C F(v)dv = 2\pi i \sum_k \mathrm{Res}\left[F(v),\ v_k\right] \qquad (37)$$

does not apply directly to our case because the integration interval $[-1,1]$ does not form a closed contour. By taking the residues, we would be unable to calculate the real part of the amplitude.

We have seen in our numerical calculations that the double poles and single poles are of equal numerical importance. We have also found that the real part of the amplitude contributes at the level of about 1/4 with respect to the imaginary part.

There is no contradiction with the result of Ref. [21], where the diffractive production of J/ψ mesons was studied, and the contribution from the real part was found to be of the same order or even larger than that of the imaginary part. The difference between the production of open and bound $c\bar{c}$ states comes from the different structure and position of poles of the matrix element, as it has already been clearly explained in [21].

IV. NUMERICAL RESULTS AND DISCUSSION

First of all, we recall the definition of the basic kinematic observables (see Fig. 1): $s = (p_e + p_p)^2$, the total invariant energy squared; $Q^2 = -k_\gamma^2$, the virtuality of the exchanged photon; $y = (k_\gamma p_p)/(p_e p_p)$, the fraction of the electron energy-momentum transferred to the photon; $z = (p_D p_p)/(k_\gamma p_p)$, the fraction of the photon energy-momentum transferred to the D^4 meson; $p_t(D^4)$ and $\eta(D^4)$, the transverse momentum and rapidity of the produced D^4 meson; $W = (k_\gamma + p_p)^2$, the center-of-mass energy of the photon-proton system; M_X, the mass of the final state hadronic system separated by a rapidity gap from the proton remnant system; $x_{I\!P} = (Q^2 + M_X^2)/sy = (Q^2 + M_X^2)/(Q^2 + W^2)$, the fraction of the proton energy transferred to the Pomeron; $x = Q^2/2(k_\gamma p_p)$, the Bjorken variable; and $\beta = x/x_{I\!P} = Q^2/(Q^2 + M_X^2)$.

In addition to that, the H1 collaboration uses the variable $z_{I\!P} = (Q^2 + s^{\rm obs})/x_p ys$. The meaning of $z_{I\!P}$ is the fraction of the Pomeron's energy-momentum carried by the interacting gluon. This definition is based on the "constituent" picture of the Pomeron (see Fig. 1, left panel), but does not suit well the two-gluon exchange model (Fig. 1, right panel). For the LO subprocess (2) $z_{I\!P}$ must be identically equal to 1; but at the NLO, it can be interpreted as the fraction of the Pomeron energy transferred to the charmed quark pair, $z_{I\!P} = \left[(p_1 k_\gamma) + (p_2 k_\gamma)\right]/(p_{I\!P} k_\gamma)$. The latter definition was used in our theoretical calculations.

The collaborations H1 and ZEUS have collected data in the photoproduction and deep-inelastic domains. The H1 photoproduction domain is defined as $Q^2 < 0.01$ GeV^2, $0.3 < y < 0.65$, $x_{I\!P} < 0.04$, $|t| < 1$ GeV^2, $p_T(D^4) > 2$ GeV, and $|\eta(D^4)| < 1.5$.

The H1 deep-inelastic domain is $2 < Q^2 < 100$ GeV^2, $0.05 < y < 0.7$, $x_{I\!P} < 0.04$, $|t| < 1$ GeV^2, $p_T(D^4) > 2$ GeV, and $|\eta(D^4)| < 1.5$.

The ZEUS photoproduction domain is $Q^2 < 1$ GeV^2, $0.17 < y < 0.89$, $130 < W < 300$ GeV, $x_{I\!P} < 0.035$, $p_T(D^4) > 1.9$ GeV, and $|\eta(D^4)| < 1.6$. Events with $x_{I\!P} < 0.01$ have been considered as a separate subsample.

The ZEUS deep-inelastic domain is $1.5 < Q^2 < 200$ GeV^2, $0.02 < y < 0.7$, $x_{I\!P} < 0.035$, $\beta < 0.8$, $p_T(D^4) > 1.5$ GeV, and $|\eta(D^4)| < 1.5$. Events with $x_{I\!P} < 0.01$ have again been considered as a separate subsample.

The parameter setting in theoretical calculations was as follows: charmed quark mass, $m_c = m_D = 1.8$ GeV; Peterson fragmentation parameter, $\epsilon(c \to D^4) = 0.06$; overall fragmentation probability, $f(c \to D^4) = 0.24$ [22]; renormalization scale in the strong coupling and factorization scale in the gluon density, $\mu_R^2 = \mu_F^2 = \hat{s}/4$.

To regulate the collinear and infrared divergences in the NLO matrix element we impose cutoffs on the invariant mass of the final state quark-gluon subsystems, $(p_1 + k_g)^2 > M_{\rm cut}^2$ and $(p_2 + k_g)^2 > M_{\rm cut}^2$, with $M_{\rm cut} = 2.5$ GeV. The physics motivation is that, if the mass of a quark-gluon system is of the order of the hadron mass, the gluon emission is under the control of confinement forces where pQCD methods are not applicable. We also require that the transverse momentum of the final state gluon be larger than 2 GeV. The sensitivity of the results to the cutoff value is logarithmic, so that increasing $M_{\rm cut}$ from 2.5 to 5 GeV has approximately a 25% decreasing effect on the production cross section.

The choice of formfactor is an important issue. Within the factorization hypothesis (8), the production cross section is proportional to the integral $\int_0^{t_{max}} r^2(t)\,dt$. Experimental data [17] give evidence for changing the value of the effective slope parameter b from $b \approx 9$ GeV^{-2} at the lowest $|t|$ to $b \approx 4.5$ GeV^{-2} at $|t| \simeq 1$ GeV^2. Another evidence is given by the diffractive production of $W^\pm$ and Z bosons at the Tevatron, showing the t dependence of cross sections like $d\sigma/dt \propto 6.38e^{-8|t|} + 0.424e^{-3|t|}$ [23]. Given the normalization condition $r^2(t{=}0) = 1$, we get from Eq. (10) $\int_0^1 r^2(t)\,dt = 0.125$, a value which is about twice as low compared to that if more ordinary parametrizations, such as $r^2(t) = \left[(4 - 2.8t)/(4 - t)\right]^2 (1 - t/0.7)^{-4}$ [24] or $r^2(t) = (1 - t/m_{2_g}^2)^{-4}$ with $m_{2_g}^2 = 0.55$ GeV^2 [25] would have been used. Taken together, the theoretical uncertainties (connected to the quark mass, factorization scale, formfactor and infrared regularization) can change the predicted cross sections by a factor of roughly 2 with respect to its central value. The uncertainties mainly concern the absolute normalization and, to a much less extent, the shape of the distributions.

Our numerical results are displayed in Figs. 4-7. In addition to the experimentally measured differential cross sections, we show predictions on the angular distribution $d\sigma/d\psi$, with ψ being the angle between the electron scattering plane and the D^4 meson production plane. We

recover the well-known LO result [26] that, in the photon-Pomeron rest frame, the produced quarks prefer to lie in the plane perpendicular to the electron scattering plane. However, the effect is washed out when the NLO contribution is considered (see Fig. 4, the right side of the lower panel).

In general, the agreement with experimental data is reasonably good. It could even be said to be surprisingly good, if not excellent, having in mind that quite a lot of different distributions at rather different kinematic regimes have been described within the same parameter setting. The only conclusion that we can derive from this fact is, maybe, just the consistency of the model.

Our approach shows agreement with the data of at least the same quality as that of Ref. [8], and it would hardly be possible to favor either of the two on the basis of the comparison with experiment. On the technical side, our approach has the advantage of enabling one to separately calculate the real and imaginary parts of the amplitude. But, on the other hand, this could be of only academic interest, because the contribution from the real part is found to be not very important numerically for the process under consideration.

We agree with the result of Ref. [6] that the production cross section in the deep-inelastic regime is dominated by the NLO rather than LO partonic subprocess, although the LO contribution is not totally negligible. At the same time, the LO contribution plays almost no role in the photoproduction regime.

V. CONCLUSION

We have considered the diffractive production of D^* mesons at HERA conditions in the framework of the two-gluon exchange model in its collinear interpretation. The same approach and the same parameter setting was applied to describe the data collected by the H1 and ZEUS collaborations in the deep-inelastic and real photoproduction regions, and a very good agreement was found in all cases. The success of the approach can be regarded as validation of its consistency.

Acknowledgments

The author thanks J.Bartels, G. Gustafson, D. Ivanov, H. Jung, I.Korzhavina, L. Motyka, and, especially, N. Zotov for valuable discussions. This work was supported by the FASI of RF (Grant No. NS-1856.2008.2), the RFBR foundation (Grant No. 08-02-00896-a), and the DESY Directorate in the framework of Moscow-DESY project on MC implementation for HERA-LHC.

[1] H1 Collab., A. Aktas *et al.*, Eur. Phys. J. C 50, 1 (2007).
[2] ZEUS Collab., S. Chekanov *et al.*, Nucl. Phys. B672, 3 (2003).
[3] ZEUS Collab., S. Chekanov *et al.*, Eur. Phys. J. C 51, 301 (2007).
[4] H. Lotter, Phys. Lett. B 406, 171 (1997).
[5] J. Bartels, H. Jung, and M. Wüsthoff, Eur. Phys. J. C 11, 111 (1999).
[6] J. Bartels, H. Jung, and A. Kyrieleis, Eur. Phys. J. C 24, 555 (2002).
[7] A. V. Berezhnoy, V. V. Kiselev, I. A. Korzhavina, and A. K. Likhoded, Phys. At. Nuclei 65, 1487 (2002).
[8] L. V. Gribov, E. M. Levin, and M. G. Ryskin, Phys. Rep. 100, 1 (1983); E. M. Levin and M. G. Ryskin, Phys. Rep. 189, 267 (1990).
[9] J. A. M. Vermaseren, Symbolic Manipulations with FORM, published by CAN (Computer Algebra Nederland), Kruislaan 413, 1098, SJ Amsterdaam 1991, ISBN 90-74116-01-9.
[10] S. P. Baranov, Phys. At. Nuclei 60, 1322 (1997); S. P. Baranov and V. L. Slad', Phys. At. Nuclei 70, 2113 (2007).
[11] X. D. Ji, Phys. Rev. D 55, 7114 (1997); J. Phys. G 24, 1181 (1998).
[12] A. V. Radyushkin, Phys. Lett. B 385, 333 (1996); A. V. Radyushkin, Phys. Rev. D 56, 5524 (1997).
[13] A. V. Radyushkin, Phys. Rev. D 59, 014030 (1998); Phys. Lett. B 449, 81 (1999).
[14] A. Freund and M. McDermott, Phys. Rev. D 65, 074008 (2002); A. Freund, M. McDermott, and M. Strikman, Phys. Rev. D 67, 036001 (2003).
[15] M. Glück, E. Reya, and A. Vogt, Eur. Phys. J. C 5, 461 (1998).
[16] K. J. Golec-Biernat, A. D. Martin, and M. G. Ryskin, Phys. Lett. B 456, 232 (1999).
[17] ZEUS Collab., J.Breitweg *et al.*, Eur. Phys. J. C 6, 603 (1999).
[18] E. Byckling and K. Kajantie, *Particle Kinematics*, (John Wiley and Sons, New York, 1973).
[19] G. P. Lepage, J. Comp. Phys. 27, 192 (1978).
[20] C. Peterson, D. Schlatter, I. Schmitt, and P. M. Zerwas, Phys. Rev. D 27, 105 (1983).
[21] S. P. Baranov, Phys. Rev. D 76, 034021 (2007).
[22] L. Gladilin, hep-ex/9912064; ZEUS Collab., S. Chekanov *et al.*, Eur. Phys. J. C 44, 351 (2005).
[23] P. Bruni and G. Ingelman, Phys. Lett. B 311, 317 (1993).
[24] A. Donnachie and P. V. Landshoff, Nucl. Phys. B 244, 322 (1984); Nucl. Phys. B 303, 634 (1988).
[25] L. Frankfurt and M. Strikman, Phys. Rev. D 66, 031502(R) (2002).
[26] J. Bartels, C. Ewerz, H. Lotter, and M. Wüsthoff, Phys. Lett. B 386, 389 (1996) and references therein.

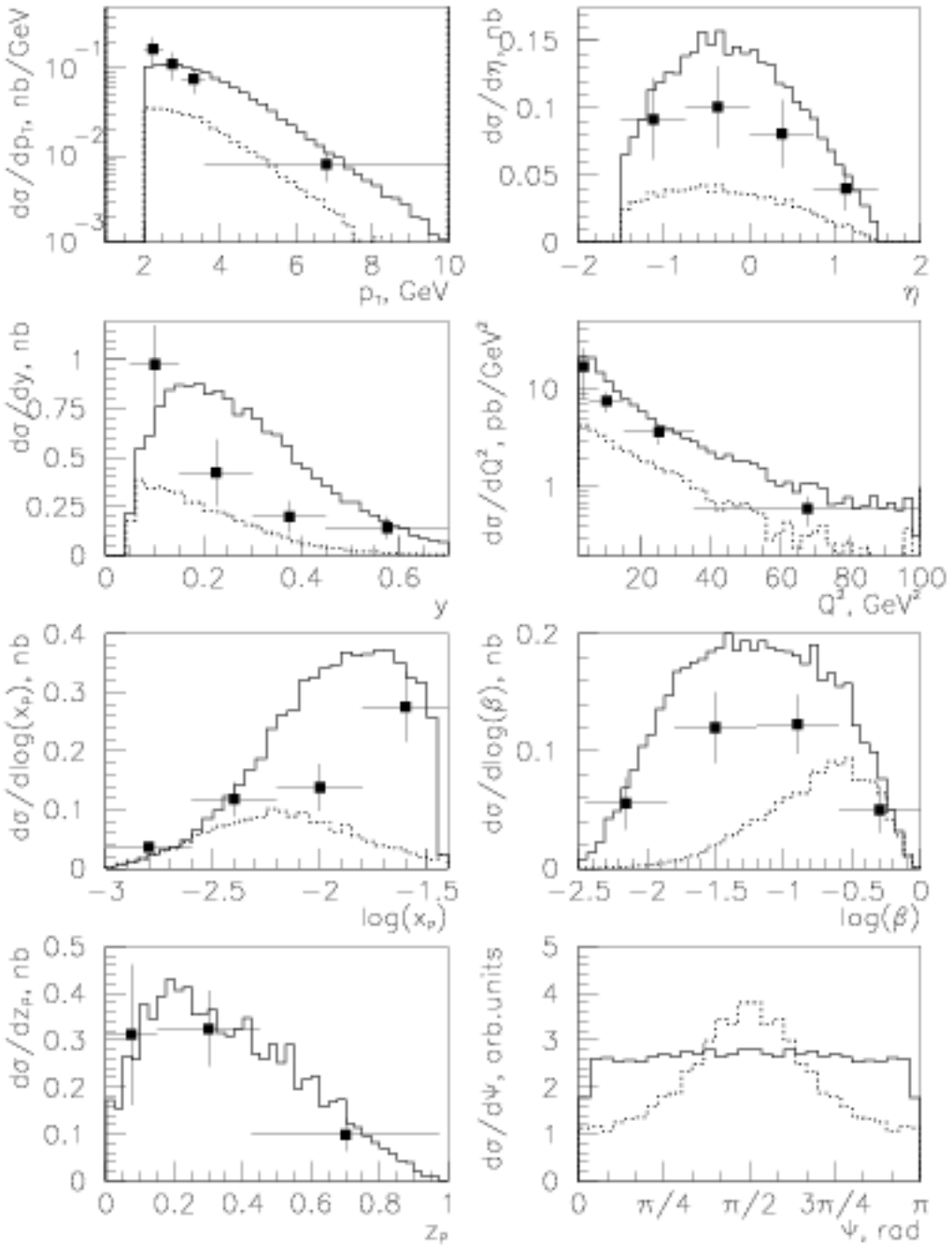

FIG. 4: Predictions on the differential cross sections within the H1 deep-inelastic kinematic range. Solid histograms show the sum of LO and NLO contributions; dotted histograms are for LO contributions alone; ■ represent H1 experimental data. The angular distributions $d\sigma/d\psi$ are shown with an arbitrary normalization for ease of comparison.

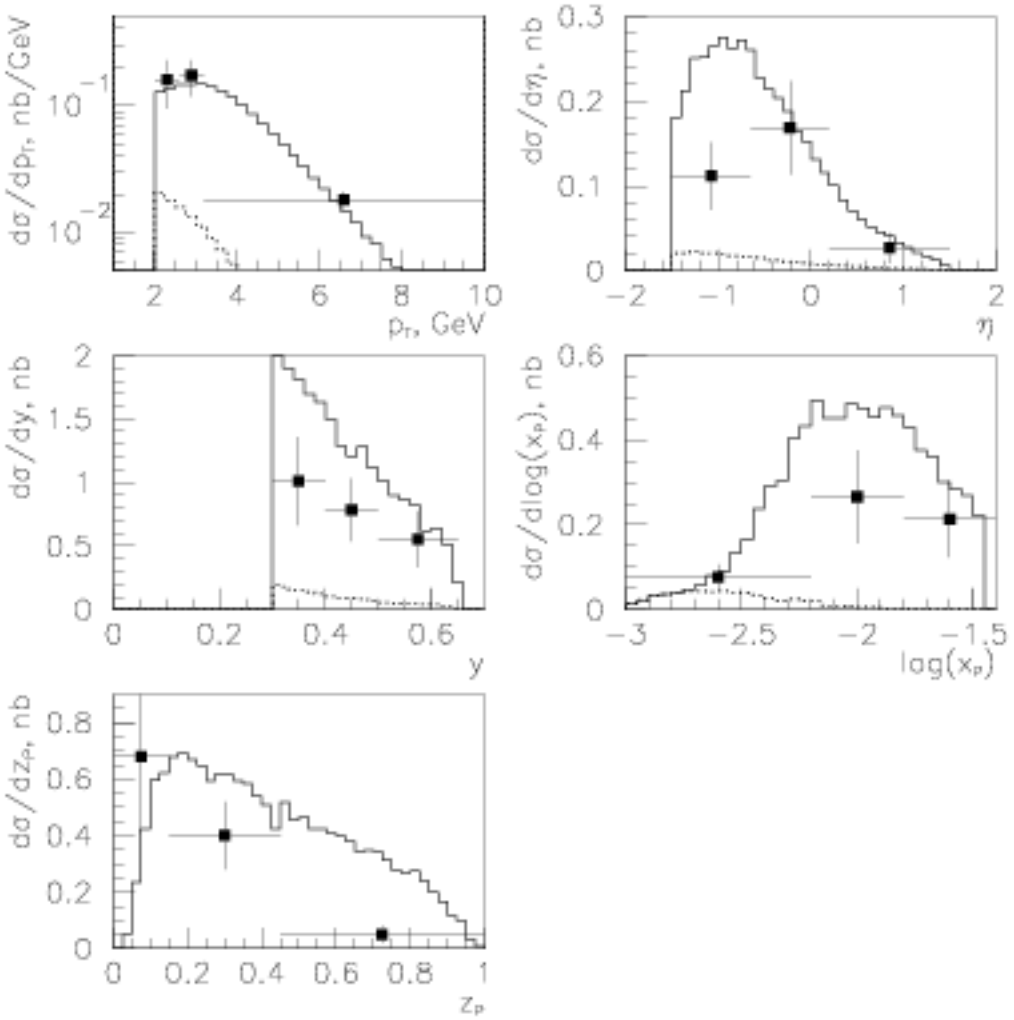

FIG. 5: Predictions on the differential cross sections within the H1 photoproduction kinematic range. Solid histograms show the sum of LO and NLO contributions; dotted histograms are for LO contributions alone; ■ represent H1 experimental data.

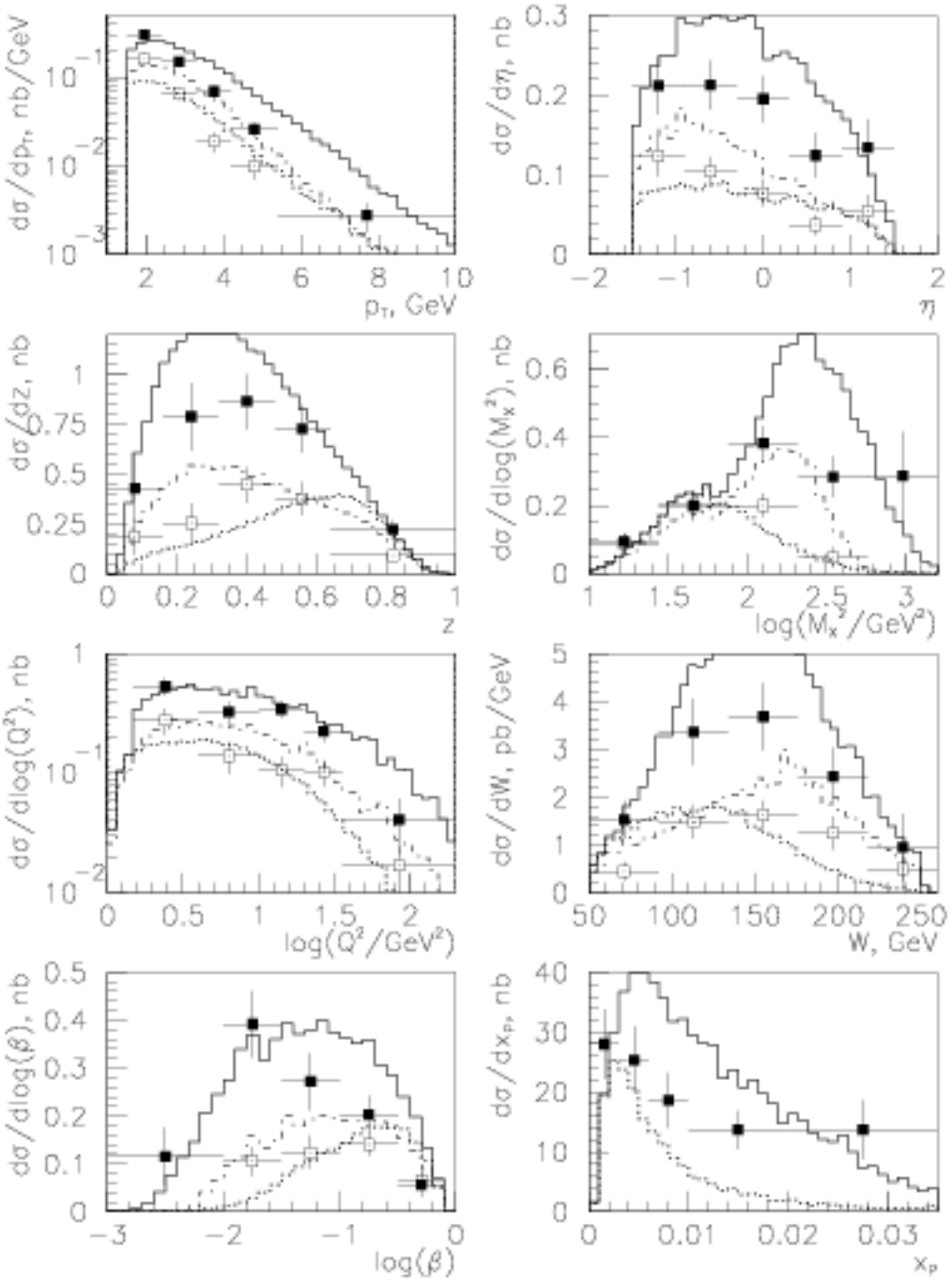

FIG. 6: Predictions on the differential cross sections within the ZEUS deep-inelastic kinematic range. Solid histograms show the sum of LO and NLO contributions for $x_{I\!P} < 0.035$; dash-dotted histograms show LO+NLO for $x_{I\!P} < 0.01$; dashed histograms, are LO contributions alone for $x_{I\!P} < 0.035$; ZEUS experimental data: ■ represent $x_{I\!P} < 0.035$; □ represent $x_{I\!P} < 0.01$.

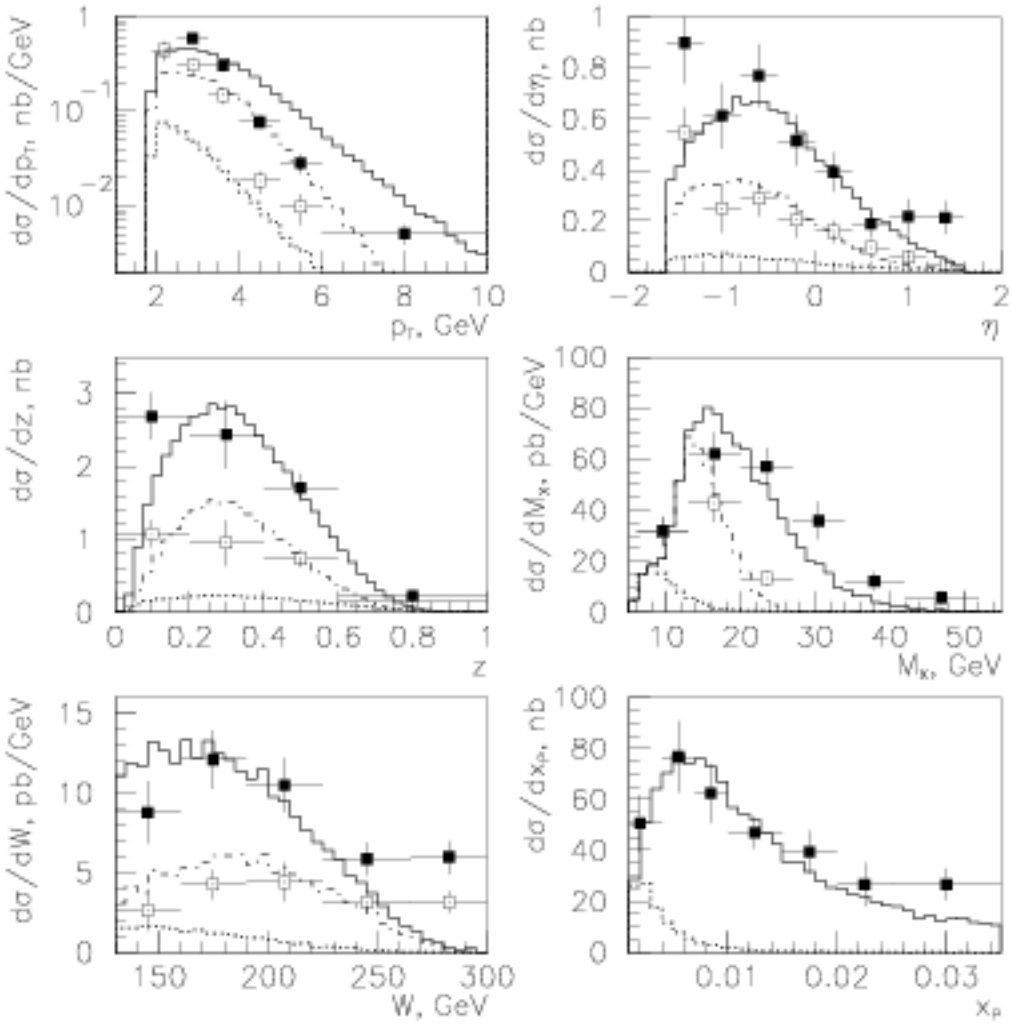

FIG. 7: Predictions on the differential cross sections within the ZEUS real photoproduction kinematic range. Solid histograms, the sum of LO and NLO contributions for $x_{I\!P} < 0.035$; dash-dotted histograms, LO+NLO for $x_{I\!P} < 0.01$; dashed histograms, LO contribution alone for $x_{I\!P} < 0.035$; ZEUS experimental data: ■ represent $x_{I\!P} < 0.035$; □ represent $x_{I\!P} < 0.01$.